SPACE-TIME REVERSAL TECHNIQUES FOR INFORMATION RETRIEVAL IN WIRELESS SENSOR NETWORKS

Thiagarajan Sivanadyan and Akbar Sayeed

Department of Electrical and Computer Engineering
University of Wisconsin - Madison
thiagars@cae.wisc.edu akbar@engr.wisc.edu

ABSTRACT

In this paper, we explore the benefits of space-time reversal (STR) techniques in the context of information retrieval in wireless sensor networks under the recently proposed Active Wireless Sensing (AWS) framework. In AWS, individual sensors are differentiated via their distinct space-time signatures and STR schemes exploit these sensor signatures. In the downlink, STR techniques are proposed to address individual sensors thus enabling sensor programming for different information retrieval or sensing modes. In the uplink, we propose an STR scheme for localizing distinct sensor responses to distinct signal space dimensions at the WIR thereby reducing interference between sensor transmissions. Furthermore, it does not require explicit estimation of sensor signatures at the WIR. The benefits of STR techniques in both scenarios are quantified analytically and illustrated with physically meaningful simulation results.

1. INTRODUCTION

Time-reversal (TR) techniques have been used extensively in several acoustic, imaging and under-water communications applications to yield significant performance gains (see, e.g., [1, 2]). Extensions of TR to wireless communication systems has gained recent attention due to their ease of implementation and ability to exploit the multipath nature of wireless channels (see, e.g., [3, 4]). In traditional communication systems, the initial training signals for channel estimation typically originate at the transmitter; however, in TR, the receiver initiates communication by sending training signals to the transmitter that can then time reverse (and phase-conjugate) its acquired waveforms to send data. Under ideal conditions, this process eliminates the channel estimation/equalization requirement at the receiver by focusing the transmitted energy in space and time at the target (receiver) location. With the emergence of TR applications in multi antenna systems, the term space-time-reversal (STR) seems more appropriate since the wireless channel now incorporates an added spatial dimension.

In this paper, we investigate STR techniques in the context of AWS [5, 6] in which a wireless information retriever (WIR) or access point, equipped with an antenna array, directly communicates with an ensemble of sensors using wideband space-time waveforms. A key idea behind our approach is that distinct sensors are associated with distinct space-time signatures induced at the WIR that can then be exploited for establishing simultaneous communication between the WIR and the entire sensor ensemble. These space-time signatures which represent the channel between individual sensors and the WIR, depend on the sensor locations, the scattering environment and the spatio-temporal signal space dimension of the interrogation waveform.

This work was partly supported by the NSF grant CNS-0627589.

STR techniques for exploiting the differences in the sensors' space-time signatures are explored in both the downlink and the uplink in AWS. In the downlink, STR techniques are proposed for sending dedicated information from the WIR to distinct sensors for programming them for different information retrieval tasks. In this case, the WIR first estimates space-time signatures for different sensors based on transmission of an identical (common) spread-spectrum waveform from each sensor. The WIR then uses space-time reversed versions of the sensor signatures as modulation waveforms, and low-complexity interference cancelation schemes at the WIR are proposed to reduce the interference between data streams aimed at distinct sensors, thereby increasing the number of sensors that can be simultaneously and reliably addressed. In the uplink, we present an STR scheme to localize distinct sensor responses at distinct signal space dimensions at the WIR thereby reducing the interference between sensor transmissions. In this case, sensors first acquire distinct temporal waveforms as a result of interrogation by the WIR with space-time waveforms localized to distinct signal space dimensions.

The next section introduces the basic system model in AWS, the multipath scattering channel and the sensor angle-delay signatures. In section 3 we present STR techniques applicable in the downlink to allow simultaneous transmissions to multiple sensors along with the associated interference suppression schemes at the WIR. Section 4 discusses an uplink STR signaling scheme for generating a space-time focused response at the WIR for each sensor. Finally in section 5, we discuss the issues related to realizing STR techniques in practice, and relevant research directions. In all sections, we present illustrative numerical results to support the analysis.

2. AWS SYSTEM MODEL

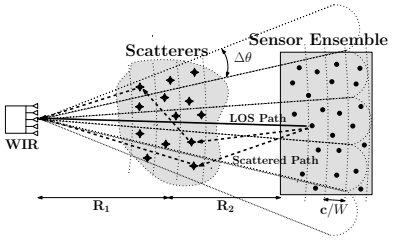

Fig. 1. AWS over a multipath scattering channel.

Consider an ensemble of K sensors randomly distributed over a region of interest, as illustrated in Fig. 1. The WIR equipped with an M-element uniform linear array (ULA), initiates information retrieval by sending a signal for timing and frequency synchroniza-

tion. The i-th sensor modulates a unit energy spread-spectrum signal $q(t)$ (known at the WIR) of duration T and bandwidth W with its (possibly encoded) measurement β_i, and transmits it with energy $\mathcal{E}$ after a fixed delay (same for all sensors). The transmitted sensor signals pass through a multipath channel consisting of N_p scattering paths (see Fig. 1). The received vector signal at the WIR, $\boldsymbol{r}(t) = [r_1(t), r_2(t), \ldots, r_M(t)]^T$, is a superposition of all the sensor transmissions

$$\boldsymbol{r}(t) = \sqrt{\mathcal{E}} \sum_{i=1}^{K} \beta_i \sum_{n=1}^{N_p} \alpha_{i,n} q(t - \tau_{i,n}) \boldsymbol{a}(\theta_{i,n}) + \boldsymbol{w}(t) \quad (1)$$

where $\tau_{i,n}$ is the relative delay, $\theta_{i,n}$ the angle of arrival (AoA), $\alpha_{i,n}$ the complex path gain of the i-th sensor's signal through the n-th scattering path, and $\boldsymbol{w}(t)$ denotes a vector AWGN process with independent components. The unit-norm ULA steering/response vector is denoted by $\boldsymbol{a}(\theta)$ where θ is the normalized angle [5]. Let $\tau_{i,n} \in [0, \tau_{max}]$ where $\tau_{max} = \max(\tau_{i,n})$ denotes the channel delay spread. Without loss of generality (WLOG), assume that for each sensor, the $n = 1$ path represents the line-of-sight (LOS) component with energy $|\alpha_{i,1}|^2 = 1$ and the remaining $N_p - 1$ paths are non-line-of-sight (NLOS) with energy $|\alpha_{i,n}|^2 = \sigma_p^2 < 1, n = 2, \ldots, N_p$, as shown in Fig. 1. Thus, the channel power $\sigma_c^2 = \sum_n |\alpha_{i,n}|^2 = 1 + (N_p - 1)\sigma_p^2$ grows linearly with N_p, since more paths couple more signal energy transmitted from the sensors to the WIR. We also assume that $\{\theta_{i,n}, \tau_{i,n}\}$ are fixed. The only source of channel randomness are the random and independent phases of the gains $\{\alpha_{i,n}\}$.

2.1. Sensor Angle-Delay Signatures

To retrieve the sensor information, the WIR performs angle-delay matched filtering - $\boldsymbol{r}(t)$ is first projected in M fixed spatial directions and then correlated with uniformly delayed versions of $q(t)$ to yield the sufficient statistics

$$z_{m,\ell} = \int_0^T \boldsymbol{a}^H(m/M) \boldsymbol{r}(t) q^*(t - \ell/W) dt \quad (2)$$

where $m = -\tilde{M}, \ldots, \tilde{M}$, $\ell = 0, \ldots, L-1$, $\tilde{M} = (M-1)/2$ and $L = \lceil \tau_{max} W \rceil$. Stacking the angle-delay matched filtered (MF) outputs in an $N_s = M \times L$ dimensional vector we have

$$\boldsymbol{z} \quad = \quad \sqrt{M\mathcal{E}} \boldsymbol{\Gamma} \boldsymbol{\beta} + \boldsymbol{w} = \sqrt{M\mathcal{E}} \sum_{i=1}^{K} \beta_i \boldsymbol{\gamma}_i + \boldsymbol{w} \quad (3)$$

where $\boldsymbol{\Gamma} = [\boldsymbol{\gamma}_1, \cdots, \boldsymbol{\gamma}_K]$ is the $N_s \times K (N_s \geq K)$ channel matrix that maps the sensor data vector, $\boldsymbol{\beta} = [\beta_1, \ldots, \beta_K]^T$, to the angle-delay MF output vector $\boldsymbol{z}$, and $\boldsymbol{w}$ is a complex AWGN vector with i.i.d. components of variance σ^2. The vector $\boldsymbol{\gamma}_i$ represents the *angle-delay signature* generated by the i-th sensor at the WIR. The contribution of the scattering paths to the sensors' angle-delay signatures is captured by the virtual path partitioning commensurate with resolution in angle and delay afforded by the signal space [5, 7]

$$\gamma_i(m, \ell) \approx \sum_{n \in S_{m,\ell}(i)} \alpha_{i,n} \quad (4)$$

where $S_{m,\ell}(i) = \{n : |\theta_{i,n} - m/M| < 1/2M \ , \ |\tau_{i,n} - \ell/W| < 1/2W\}$ is the set of all paths associated with the i-th sensor whose angles and delays lie within the *angle-delay resolution bin* of size $\Delta\theta \times \Delta\tau = (1/M) \times (1/W)$ associated with the (m, ℓ)-th angle-delay MF output in (2). It follows from (4) that in a multipath environment with sufficiently many and spatially distributed NLOS paths, $\boldsymbol{\gamma}_i$ exhibits a large number of dominant non-vanishing components or degrees of freedom (DoF) that are *statistically independent* since disjoint sets of paths (with independent phases) contribute to distinct components. Note that both the number of DoF and the average energy in each signature, $\mathrm{E}\left[\|\boldsymbol{\gamma}_i\|^2\right] = \sigma_c^2$ grow with N_p [6].

3. AWS DOWNLINK: SPACE-TIME REVERSAL TO ADDRESS INDIVIDUAL SENSORS

One of the attractive features of AWS is the ability of the WIR to "program" the sensors for different tasks which requires that the WIR be able to individually address different sensors. In this section, we propose a simple STR signaling scheme at the WIR that exploits the differences in the sensor signatures for simultaneously addressing individual sensors, *without* knowing their locations, and without the need for channel estimation at the sensors. Our results show that the richer the multipath, the sharper the ability to focus the signal at a desired sensor while minimizing the interference to other sensors. The downlink STR scheme requires knowledge of $\boldsymbol{\Gamma}$ at the WIR. We assume perfect knowledge of $\boldsymbol{\Gamma}$, although in practice it has to be estimated with training signals from sensors.

3.1. System Model

Let $b_i \in \{-1, +1\}$ represent the information symbol for the i-th sensor. Then the STR signal transmitted from the WIR intended for the i-th sensor is given by

$$\boldsymbol{s}_{tr,i}(t) = \sqrt{\frac{\mathcal{E}}{c_1}} \sum_{\ell,m} b_i \gamma_i^*(m, \ell) \boldsymbol{a}^* \left(\frac{m}{M}\right) q^* \left(\tilde{T} - t - \frac{\ell}{W}\right) \quad (5)$$

where $0 \leq t \leq \tilde{T}$, $\tilde{T} = T + \tau_{max}$, $c_1 = \|\boldsymbol{\gamma}_i\|^2$ and the normalization ensures that the transmitted signal has energy $\mathcal{E}$. The received TR signal at the k-th sensor is

$$r_{tr,k}(t) \quad = \quad \sum_{n=1}^{N_p} \alpha_{k,n} \boldsymbol{a}^T(\theta_{k,n}) \boldsymbol{s}_{tr,i}(t - \tau_{k,n}) + w(t) \quad (6)$$

where $w(t)$ denotes an AWGN process. The received signal $r_{tr,k}(t)$ is matched filtered at the k-th sensor with $q(t)$ and the corresponding MF output at time τ is

$$z_{tr,k}(\tau) = \int r_{tr,k}(t) q(\tau - t) dt \quad (7)$$

$$= \sqrt{\frac{\mathcal{E}}{c_1}} b_i \sum_{\ell,m,n} \alpha_{k,n} \gamma_i^*(m, \ell) \boldsymbol{a}^T(\theta_{k,n}) \boldsymbol{a}^* \left(\frac{m}{M}\right) \int q^* \left(\tilde{T} - t + \tau_{k,n} - \frac{\ell}{W}\right) q(\tau - t) dt + w(\tau) \quad (8)$$

where $w(\tau)$ is complex Gaussian noise with variance σ^2. The received SNR at the target (i-th) sensor is maximized at $\tau = \tilde{T}$ and the MF output at the k-th sensor at this 'optimum' time can be shown, using virtual path partitioning (4) to be [6]

$$z_{tr,k}(\tilde{T}) = \sqrt{\frac{\mathcal{E}}{c_1}} \boldsymbol{\gamma_k}^T \boldsymbol{\gamma_i^*} b_i + w(\tilde{T}) \quad (9)$$

Thus, at the optimal sampling time, the SNR at the k-th sensor is $\frac{\mathcal{E}|\boldsymbol{\gamma}_k^T \boldsymbol{\gamma}_i^*|^2}{\sigma^2 \|\boldsymbol{\gamma}_i\|^2}$ which is maximum at the target sensor ($k = i$). This is illustrated in Fig. 2 which plots the value of the SNR at different sensors. The accompanying image plot corresponds to magnitude of the MF output $|z_{tr,k}(\tilde{T})|^2$. Note that with increasing N_p, the SNR of the received TR signal increases at the target sensor, whereas it decreases at the other sensors. This is because of the increasing number of DoF and higher energy in the signature vectors (see Sec. 2.1).

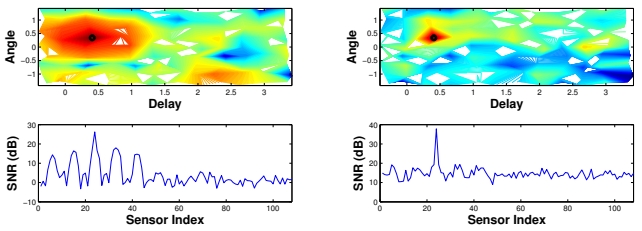

(a) (b)

Fig. 2. The strength of the received TR signal at different sensors for different values of N_p; a black circle indicates the target sensor (sensor 24) in the image plots; $K = 108$; $\sigma_p^2 = 1/8$, $M = 9$, $L = 12$ and $N_s = ML = 108$ are used for all the numerical results in this paper. (a) $N_p = 20$. (b) $N_p = 100$.

If all the sensors are addressed simultaneously, we can show that the STR MF outputs at the sensors $\boldsymbol{z}_{tr} = [z_{tr,1}(\tilde{T}), \ldots, z_{tr,K}(\tilde{T})]^T$ are given by

$$\boldsymbol{z}_{tr} = \sqrt{\frac{\mathcal{E}}{\mathrm{tr}(\boldsymbol{\Gamma}^H\boldsymbol{\Gamma})}}\boldsymbol{\Gamma}^T\boldsymbol{\Gamma}^*\boldsymbol{b} + \boldsymbol{w} \tag{10}$$

where $\boldsymbol{b} = [b_1, \ldots, b_K]^T$ and $\boldsymbol{w}$ denotes an AWGN vector. Thus, the SINR at the i-th sensor can then be written as

$$\mathrm{SINR}(i) = \frac{\mathcal{E}\|\boldsymbol{\gamma}_i\|^4/c_1}{\sigma^2 + \mathcal{E}\sum_{k\neq i}|\boldsymbol{\gamma_k}^T\boldsymbol{\gamma_i}^*|^2/c_1} \tag{11}$$

and using the Gaussian approximation for interference, the probability of error in the estimated bit $\hat{b}_i = \mathrm{sign}(\mathrm{Re}\{z_{tr,i}(\tilde{T})\})$ is given by $P_e(i) = \mathrm{Q}(\sqrt{2\mathrm{SINR(i)}})$. In general, since the instantaneous realizations of the signatures are not orthogonal $|\boldsymbol{\gamma_k}^T\boldsymbol{\gamma_i}^*|^2 \neq 0$, this STR signaling scheme is interference limited since the SINR and the P_e saturate as the transmit SNR ($\mathcal{E}/\sigma^2$) is increased

$$\mathrm{SINR}(i) \rightarrow \frac{\mathcal{E}\|\boldsymbol{\gamma}_i\|^4}{\sum_{k\neq i}|\boldsymbol{\gamma_k}^T\boldsymbol{\gamma_i}^*|^2} \text{ as } \frac{\mathcal{E}}{\sigma^2} \rightarrow \infty\,. \tag{12}$$

This saturation behavior of the SINR and P_e is illustrated in Fig. 3. Note that although increasing the amount of scattering (larger N_p) can initially increase (decrease) the saturation threshold of the SINR (P_e), it provides diminishing returns.

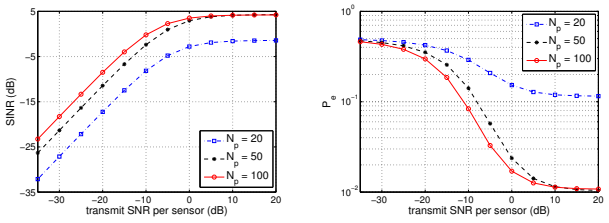

(a) (b)

Fig. 3. (a) SINR vs per-sensor transmit SNR ($\mathcal{E}/K\sigma^2$) when $K = 54$ sensors are simultaneously addressed. (b) The corresponding P_e vs SNR. All the SINR and P_e curves in this paper represent the average over all the sensors and multiple channel phase realizations.

3.2. Interference suppression at the WIR

As evident from Fig. 3, the P_e for the basic STR signaling suffers from an error floor due to the interference between the different sensor transmissions. Since the communication channel between the WIR and the sensor ensemble is equivalent to a semi-distributed multiple input multiple output (MIMO) broadcast channel, a number of low-complexity linear MIMO transmit processing techniques can be leveraged to combat this interference. In this section, we discuss one particular interference suppression scheme at the WIR, the transmit Wiener filter (WF) [8]. Let the $N_s \times K$ matrix $\boldsymbol{G}$ denote the WIR transmit pre-filter that maps $\boldsymbol{b}$ to the downlink channel $\boldsymbol{\Gamma}^T$. Then the STR MF outputs at the K sensors are given by

$$\boldsymbol{z}_{tr} = \boldsymbol{\Gamma}^T\boldsymbol{G}\boldsymbol{b} + \boldsymbol{w}\,. \tag{13}$$

Note from (10) that the basic STR signaling scheme corresponds to $\boldsymbol{G} = \sqrt{\frac{\mathcal{E}}{\mathrm{tr}(\boldsymbol{\Gamma}^H\boldsymbol{\Gamma})}}\boldsymbol{\Gamma}^*$. The WF with energy constraint $\mathcal{E}$ is designed to minimize a *modified* mean-squared error at the individual sensors:

$$\begin{aligned}\{\boldsymbol{G}_{WF}, \delta_{WF}\} &= \mathrm{argmin}_{\{\boldsymbol{G},\delta\}}\mathrm{E}\left[\|\delta^{-1}\boldsymbol{z}_{tr} - \boldsymbol{b}\|^2\right] \\ \text{s.t.}: \mathrm{tr}\left(\boldsymbol{G}^H\boldsymbol{G}\right) &= \mathcal{E}\end{aligned} \tag{14}$$

where δ denotes the gain of the filter $\boldsymbol{G}$. The optimum filter is [8]

$$\boldsymbol{G}_{WF} = \delta_{WF}\boldsymbol{F}^{-1}\boldsymbol{\Gamma}^* \text{ and } \delta_{WF} = \sqrt{\frac{\mathcal{E}}{\mathrm{tr}\left(\boldsymbol{F}^{-2}\boldsymbol{\Gamma}^*\boldsymbol{\Gamma}^T\right)}} \tag{15}$$

where $\boldsymbol{F} = \boldsymbol{\Gamma}^*\boldsymbol{\Gamma}^T + \frac{\sigma^2 K}{\mathcal{E}}\boldsymbol{I}$. In (15), $\boldsymbol{F}^{-1}$ suppresses the interference between the different sensors' signatures and the channel $\boldsymbol{\Gamma}^T$ acts as the matched filter on pre-filtered WIR signal.

The i-th sensor's MF output $z_{tr,i}$ can now be expressed as

$$z_{tr,i} = \delta_{WF}\boldsymbol{\gamma}_i^T\boldsymbol{F}^{-1}\boldsymbol{\gamma}_i^*b_i + \delta_{WF}\sum_{k\neq i}\boldsymbol{\gamma}_i^T\boldsymbol{F}^{-1}\boldsymbol{\gamma}_k^*b_k + \boldsymbol{w} \tag{16}$$

where $\boldsymbol{\gamma}_i^T\boldsymbol{F}^{-1}\boldsymbol{\gamma}_i^*$ represents the filtered desired signal and $\boldsymbol{\gamma}_i^T\boldsymbol{F}^{-1}\boldsymbol{\gamma}_k^*$ the suppressed interference due to the k-th sensor's information stream. The P_e for the i-th bit stream can be expressed as $P_{e,WF}(i) = Q\left(\sqrt{2\mathrm{SINR}_{WF}(i)}\right)$ where

$$\mathrm{SINR}_{WF}(i) = \frac{\delta_{WF}|\boldsymbol{\gamma}_i^T\boldsymbol{F}^{-1}\boldsymbol{\gamma}_i^*|^2}{\sigma^2 + \delta_{WF}\sum\limits_{k\neq i}|\boldsymbol{\gamma}_i^T\boldsymbol{F}^{-1}\boldsymbol{\gamma}_k^*|^2} \tag{17}$$

We note that the P_e associated with Wiener filtering does not suffer from error floors [8] as confirmed by the numerical results presented in Fig. 4. For larger N_p, both the increase in the number of DoF and higher energy in $\boldsymbol{\gamma}_i$ (see Sec. 2.1) contribute to better P_e performance. The diversity increase is illustrated in Fig. 4(a) where the energy in the $\{\gamma_i\}$ is kept constant for varying N_p, whereas Fig. 4(b) captures both these effects.

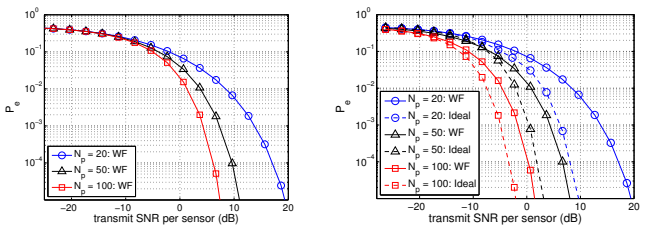

(a) (b)

Fig. 4. P_e vs per-sensor transmit SNR ($\mathcal{E}/K\sigma^2$) with transmit Wiener filtering; $K = 108$. (a) Constant total channel energy. (b) Channel energy increases with N_p (energy capture); the ideal curves represent the interference-free P_e.

4. SPACE-TIME REVERSAL IN AWS UPLINK

In the basic AWS uplink signaling architecture expressed in (3), decoding the sensor data $\boldsymbol{\beta}$ from the received MF outputs $\boldsymbol{z}$ requires reliable estimates of $\boldsymbol{\Gamma}$, the signature matrix, which are obtained in practice by sending training signals from the sensors. In particular for coherent signaling, the training cost on sensor energy for accurate phase estimates can be high. In this section, we discuss an alternate STR scheme for uplink communication that eliminates this estimation requirement by focusing sensor responses at desired signal space locations at the WIR. In this case, the WIR initiates the information retrieval by sending high powered interrogation waveforms that are localized to distinct angle-delay bins. The resulting sensor responses and the corresponding MF outputs at the WIR are focused in distinct angle-delay bins in contrast to $\{\boldsymbol{\gamma}_i\}$ which are dispersed in angle and delay.

Assume that we want to focus the i-th sensor's signal in the $(m(i), \ell(i))$-th angle delay bin. The initial transmitted signal at the WIR is given by $\boldsymbol{s}(t) = \sqrt{\mathcal{E}}\boldsymbol{a}\left(\frac{m(i)}{M}\right) q(t)$ where $\mathcal{E}$ denotes the energy of the transmitted signal. For sufficiently high $\mathcal{E}$ we can ignore noise in the downlink and hence the received signal at the i-th sensor, $r_i(t) = \sum_{n=1}^{N_p} \alpha_{i,n} \boldsymbol{a}^T(\theta_{i,n}) \boldsymbol{s}(t - \tau_{i,n})$ and the MF outputs corresponding to delays of $q(t)$ are

$$z_{i,\ell'} = \int_0^T r_i(t) q^*\left(t - \frac{\ell'}{W}\right) dt \overset{(a)}{=} \sqrt{\mathcal{E}}\gamma_i(m(i), \ell') \qquad (18)$$

where $\ell' = 0, \ldots, L-1$ and (a) follows from (4). The TR signal transmitted from the i-th sensor is now given by

$$x_{i,tr}(t) = \sqrt{\frac{\mathcal{E}}{c_2}} \beta_i \sum_{\ell'=0}^{L-1} \gamma_i^*(m(i), \ell') q^*\left(\tilde{T} - t - \frac{(\ell' - \ell(i))}{W}\right) \qquad (19)$$

where the energy normalization term $c_2 = \sum_{\ell'=0}^{L-1} |\gamma_i(m(i), \ell')|^2$ and $\ell(i)$ is the timing offset. The resulting STR received signal at the WIR, $\boldsymbol{y}_{i,tr}(t) = \sum_{n=1}^{N_p} \alpha_{i,n} \boldsymbol{a}(\theta_{i,n}) x_{i,tr}(t - \tau_{i,n}) + \boldsymbol{w}(t)$ and the corresponding ML angle-delay MF outputs are

$$\begin{aligned} z_{m,\ell} &= \sqrt{\frac{\mathcal{E}}{c_2}} \int_0^T \boldsymbol{a}^H\left(\frac{m}{M}\right) \boldsymbol{y}_{i,tr}(t) q\left(t - \frac{\ell}{W}\right) dt \qquad (20) \\ &= \sqrt{\frac{M\mathcal{E}}{c_2}} \beta_i \underbrace{\sum_{\ell'=0}^{L-1} \gamma_i^*(m(i), \ell' - \ell(i)) \gamma_i(m, \ell' - \ell)}_{\gamma_{str,i}(m,\ell)} + w_{m,\ell} \end{aligned}$$

where $\boldsymbol{w}(t)$ and $w_{m,\ell}$ denote AWGN of variance σ^2. Thus the MF output at the desired angle-delay bin, $z_{m(i),\ell(i)}$, has the maximum SNR. This is also illustrated in Fig. 5(a) which plots the SNR of the MF outputs at the WIR when $(m(i), \ell(i)) = (0, 4)$.

In order to simultaneously receive signals from multiple sensors, STR signaling can be used as long as transmissions from distinct sensors correspond to either distinct delays $\{\ell(i)\}$ (requires synchronization between sensors) or distinct angles $\{m(i)\}$ (requires distinct WIR training waveforms). In this case, the WIR MF output vector $\boldsymbol{z} = \text{vec}\{z_{m,\ell}\}$ due to K sensor uplink transmissions can be expressed as

$$\boldsymbol{z} = \sqrt{\frac{M\mathcal{E}}{c_2}} \sum_{i=1}^{K} \boldsymbol{\gamma}_{str,i} \beta_i + \boldsymbol{w} \qquad (21)$$

where $\boldsymbol{\gamma}_{str,i} = \text{vec}\{\gamma_{str,i}(m, \ell)\}$. In principle, since the $\{\boldsymbol{\gamma}_{str,i}\}$ are dominant in distinct delays or angles, the β_i can be decoded from the corresponding entries in $\boldsymbol{z}$. However, when sensor transmissions are separated by fewer angle delay bins, the interference between them can be significant as shown in Fig. 5(b). In this case, several blind source separation techniques (see, e.g., [9]) can be successfully leveraged to yield competitive performance.

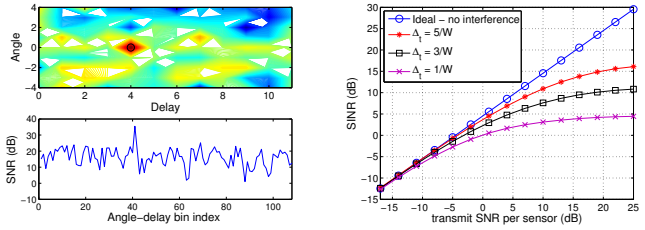

(a) (b)

Fig. 5. (a) The strength of the received TR signal at different angle delay bins; a black circle indicates the target angle-delay bin in the image plots. (b) Transmit SNR per-sensor ($\mathcal{E}/\sigma^2$) vs SINR for different time delays $\Delta_t = \min(\ell(i) - \ell(k))$ between the $K = 54$ sensor transmissions ($m(i) = 0$). For both (a) and (b), $N_p = 100$.

5. DISCUSSION AND CONCLUSIONS

This paper presents promising initial results that illustrate the benefits of STR in downlink and uplink communication in AWS. It is apparent that these results are also applicable to any general asymmetric point to multipoint communication setting. Some of the issues that warrant further investigation are discussed below. First, since we assume either noise-free STR in uplink or perfect knowledge of $\boldsymbol{\Gamma}$ in downlink, analysis of the impact of noise and/or estimation errors on the performance of STR techniques would be useful for practical implementation. Next, quantifying the effect of the richness of multipath and signal space parameters (M,W,T) on STR signaling performance has important implications in the context of adaptive signaling and agile transceivers. We also believe that extending STR techniques to spectrum sensing applications in cognitive radio (CR) and secure authentication protocols in networks would be fruitful.

6. REFERENCES

[1] M. Fink, "Time reversed acoustics," *Physics Today*, Mar 1997.

[2] R. K. Ing and M. Fink, "Time-reversed lamb waves," *IEEE Trans. Ultrasonics, Ferroelectrics, and Freq. Control*, Jul 1998.

[3] C. Oestges et al., "Time reversal techniques for broadband wireless communication systems," in *European Microwave Week*, Oct 2004.

[4] Y. Jin, Y. Jiang, and J. M. F. Moura, "Multiple antenna time reversal transmission in ultra-wideband communications," in *Proc. IEEE GLOBECOM 2007*.

[5] T. Sivanadyan and A. Sayeed, "Active wireless sensing for rapid information retrieval in sensor networks," in *Proc. IPSN 2006*.

[6] T. Sivanadyan and A. Sayeed, "Active wireless sensing in multipath environments," in *Proc. IEEE SSP 2007*.

[7] A. Sayeed, "Deconstructing multi-antenna fading channels," *IEEE Trans. Signal Processing*, Oct 2002.

[8] M. Joham, W. Utschick, and J. A. Nossek, "Linear transmit processing in MIMO communications systems," *IEEE Trans. Signal Processing*, Aug 2005.

[9] J. F. Cardoso, "Blind signal separation: statistical principles," *Proc. IEEE*, Oct 1998.